THE JOURNAL OF BIOLOGICAL CHEMISTRY VOL. 284, NO. 10, pp. 6446–6454, March 6, 2009
© 2009 by The American Society for Biochemistry and Molecular Biology, Inc. Printed in the U.S.A.

Solution Structure of the $Na_V1.2$ C-terminal EF-hand Domain*[S]

Received for publication, September 24, 2008, and in revised form, December 16, 2008 Published, JBC Papers in Press, January 7, 2009, DOI 10.1074/jbc.M807401200

Vesselin Z. Miloushev[‡], Joshua A. Levine[§], Mark A. Arbing[¶1], John F. Hunt[¶2,3], Geoffrey S. Pitt[‖2], and Arthur G. Palmer III[‡4]

From the Departments of [‡]Biochemistry and Molecular Biophysics and [§]Pathology, Columbia University, New York, New York 10032, [¶]Department of Biological Sciences, Columbia University, New York, New York 10027, and [‖]Department of Medicine, Division of Cardiology, Duke University Medical Center, Durham, North Carolina 27710

Voltage-gated sodium channels initiate the rapid upstroke of action potentials in many excitable tissues. Mutations within intracellular C-terminal sequences of specific channels underlie a diverse set of channelopathies, including cardiac arrhythmias and epilepsy syndromes. The three-dimensional structure of the C-terminal residues 1777–1882 of the human $Na_V1.2$ voltage-gated sodium channel has been determined in solution by NMR spectroscopy at pH 7.4 and 290.5 K. The ordered structure extends from residues Leu-1790 to Glu-1868 and is composed of four α-helices separated by two short anti-parallel β-strands; a less well defined helical region extends from residue Ser-1869 to Arg-1882, and a disordered N-terminal region encompasses residues 1777–1789. Although the structure has the overall architecture of a paired EF-hand domain, the $Na_V1.2$ C-terminal domain does not bind Ca^{2+} through the canonical EF-hand loops, as evidenced by monitoring ^1H,^{15}N chemical shifts during a Ca^{2+} titration. Backbone chemical shift resonance assignments and Ca^{2+} titration also were performed for the $Na_V1.5$ (1773–1878) isoform, demonstrating similar secondary structure architecture and the absence of Ca^{2+} binding by the EF-hand loops. Clinically significant mutations identified in the C-terminal region of Na_V1 sodium channels cluster in the helix I-IV interface and the helix II-III interhelical segment or in helices III and IV of the $Na_V1.2$ (1777–1882) structure.

Voltage-gated sodium channels (VGSCs)[5] are molecular assemblies that span the plasma membrane of excitable cells and conduct sodium current selectively in response to depolarizing stimuli. Mutations in VGSCs underlie a variety of diseases, including the cardiac arrhythmogenic Long-QT3 and Brugada syndromes (1, 2) and neurological syndromes, such as epilepsy (3, 4).

Known components of VGSCs include a pore-forming α subunit, auxiliary β subunits, and associated modulating proteins, such as calmodulin (5, 6). The α subunit is composed of four homologous six-transmembrane helical domains connected by inter-domain linkers and N-terminal and C-terminal cytoplasmic regions. Specific α subunit isoforms are expressed differentially in skeletal muscle ($Na_V1.4$), cardiac muscle ($Na_V1.5$) and the nervous system ($Na_V1.1$, $Na_V1.2$, $Na_V1.3$, splice variants of $Na_V1.5$, and $Na_V1.6$-$Na_V1.9$) and control the rapid upstroke of action potentials (7).

VGSC activity is characterized by two open states and several inactivated states (8). Kinetics of channel inactivation occur on timescales ranging from milliseconds to seconds and determine multiple aspects of action potentials (9, 10). The molecular mechanisms of VGSC inactivation are complex and involve the α subunit, the β subunits, and calmodulin (11–13). Specific contributions to α subunit inactivation have been localized to interhelical intra-domain regions (14–16), the linker region between domains III-IV, which forms the pore occluding inactivation gate (17, 18), and the C-terminal cytoplasmic domain (CTD) (19–21).

Specific disease-causing mutations within the CTD affect channel function by altering kinetics of channel inactivation (22). The CTD is predicted by sequence analysis (23, 24) and homology modeling (25–27) to contain a paired EF-hand domain and was observed to contain a distal calmodulin binding IQ motif (4, 12, 28–31). Structural modeling also predicts that specific interactions between helix I and helix IV control channel inactivation (27, 32). A recent model, based on NMR chemical shift perturbations, fluorescence spectroscopy, and electrophysiology, suggests that inactivation is regulated by Ca^{2+} binding to the proximal EF-hand, which is strongly influenced in turn by interactions with the distal IQ motif and cal-

* This work was supported, in whole or in part, by National Institutes of Health Grants R01 HL71165 (to G. S. P.), MSTP 5T32 GM07367 (to V. Z. M.), and R01 GM59273 (to A. G. P.). The costs of publication of this article were defrayed in part by the payment of page charges. This article must therefore be hereby marked "*advertisement*" in accordance with 18 U.S.C. Section 1734 solely to indicate this fact.

[S] The on-line version of this article (available at http://www.jbc.org) contains supplemental Table I and Figs. S1–S3.

The atomic coordinates and restraints list (code 2kav) have been deposited in the Protein Data Bank, Research Collaboratory for Structural Bioinformatics, Rutgers University, New Brunswick, NJ (http://www.rcsb.org/).

Complete resonance assignments for $Na_V1.2$ CTD (BMRB 16032) and backbone resonance assignments for $Na_V1.5$ CTD (BMRB 16031) have been deposited in the BioMagResBank.

[1] A Fellow of the Canadian Cystic Fibrosis Foundation. Present address: UCLA-DOE Institute for Genomics and Proteomics, UCLA, Los Angeles, CA 90095-1570.

[2] Established Investigators of the American Heart Association.

[3] Supported by National Institutes of Health Protein Structure Initiative Grants P50GM62413 and U54GM074958 to the Northeast Structural Genomics Consortium.

[4] A member of the New York Structural Biology Center (supported by National Institutes of Health Grant GM66354). To whom correspondence should be addressed: 701 West 168th St., Box 36, New York, NY 10032-3702. E-mail: agp6@columbia.edu; Tel.: 212-305-8675; Fax: 212-305-6949.

[5] The abbreviations used are: VSGC, voltage-gated sodium channel; Na_V1, VSGC type 1; CTD, C-terminal domain; LQT3, Long QT syndrome type 3; CaM, calmodulin; HSQC, heteronuclear single quantum spectroscopy; NOESY, nuclear Overhauser effect (NOE) spectroscopy.

modulin (33). Nevertheless, whether Ca^{2+} binds specifically to the putative CTD EF-hand and any resultant contribution to channel regulation is controversial (12, 26, 31, 34).

EXPERIMENTAL PROCEDURES

Constructs of the $Na_v1.2$ CTD were designed by limited proteolysis and H/D exchange experiments. Briefly, the CTD of $Na_v1.2$, residues 1777–1937 with the amino acid substitutions I1877A/Q1878A and an N-terminal His_6 tag MGSSHHHH-HHSSGLVPRGSHMAS (31), was subjected to proteolytic digestion with proteinase K at 4 °C for 15–60 min using a protein:protease ratio of 50:1–100:1. The termini of the protected proteolytic fragments were mapped by matrix-assisted laser desorption ionization time-of-flight time-of-flight mass spectrometry and N-terminal sequencing. H/D exchange experiments were performed by ExSAR (Monmouth Junction, NJ) and showed protection for proteolytic fragments extending from residues 1789 to 1879. The construct encompassing residues 1777–1882 of the $Na_v1.2$ CTD defined by the above experiments, including the N-terminal His tag, was used for structure determination by solution NMR spectroscopy.

[U-^{13}C,U-^{15}N] $Na_V1.2$ CTD (1777–1882) was overexpressed in *Escherichia coli* (BL21 DE3) transformed with a pET28 vector (EMD Biosciences) using M9 minimal media prepared with $^{15}NH_4Cl$ and [$^{13}C_6$]glucose (35). Cultures were grown at 37 °C to $A_{600\,nm} = 0.7$, induced with 0.5 mM isopropyl β-D-1-thiogalactopyranoside, transferred to 16 °C, and harvested after 72 h. Cells were lysed using a French press, and the $Na_V1.2$ CTD was purified with Ni^+-affinity, gel-filtration (Superdex 200), and ion-exchange (Mono Q 5/50 GL) chromatography (GE Healthcare). The N-terminal tag was not removed. Sample buffer consisted of 20 mM d_{11}-Tris (pH 7.4), 100 mM d_5-glycine, 0.1 mM d_{16}-EDTA, 1 mM d_{10}-DTT, 0.02% NaN_3, and 10% D_2O. Proteins were exchanged into this buffer using centrifugal concentrators (Amicon Inc.), flash-frozen in liquid N_2, and stored at −80 °C. Samples for calcium titrations were subsequently exchanged into 20 mM d_{11}-Tris (pH 7.4), 100 mM d_5-glycine, 10 μM d_{16}-EDTA, 1 mM d_{10}-dithiothreitol, 0.02% NaN_3, and 10% D_2O. Protein concentrations of 0.5 and 0.2 mM were used for structural experiments and calcium titrations, respectively. The $Na_V1.5$ CTD construct, residues 1773–1878, was designed by sequence alignment to $Na_V1.2$, using bl2seq (36), and protein samples were prepared by the same protocol. Sample temperatures were calibrated using 99.8% MeOD to a splitting of 1.616 ppm for $Na_V1.2$ (290.5 K) and 1.545 ppm $Na_V1.5$ (298.0 K) (37).

Backbone assignments for the $Na_V1.2$ and $Na_V1.5$ CTDs were obtained with HNCO, HNCA, HNCACB, HNCOCA, HNCACO, and CBCA(CO)NH experiments; side-chain assignments for $Na_V1.2$ CTD were obtained with HBHA(CBCACO)NH and HCCH-two-dimensional total correlation spectroscopy (TOCSY) experiments (38). A 10% ^{13}C sample was used for stereospecific assignment of Leu and Val methyl groups (39). NOE connectivities were obtained with ^{15}N-NOESY-HSQC (80-ms mixing time), $^{13}C^{aliphatic}$-NOESY-HSQC (100 ms), and $^{13}C^{aromatic}$-NOESY-HSQC (80 ms). Residual dipolar coupling constants were measured in a sample containing 15 mg/ml Pf1 phage (Asla Biotech) using two-dimensional In-phase/Antiphase ^{1}H,^{15}N HSQC for ^{1}H,^{15}N (40), three-dimensional HNCO for $^{13}C'$-$^{13}C^{\alpha}$ (41), quantitative three-dimensional HNCO for ^{15}N-$^{13}C'$ (42), and HCACO for $^1H^{\alpha}$-$^{13}C^{\alpha}$ residual dipolar coupling constants (43). Fitting of the ^{15}N-$^{13}C'$ coupling constants was performed with Mathematica v5.2 (Wolfram Research, Inc.). Chemical shifts were referenced using DSS (44).

An initial structure of $Na_V1.2$ CTD was calculated from dihedral angle and NOE distance restraints, with several iterations to resolve ambiguity using ARIA 2.2 (45) and CNS 1.2 (46). The structure was refined with XPLOR-NIH 2.18 using dihedral angle, NOE distance, and residual dipolar coupling constants restraints (47, 48). Dihedral angle restraints were derived from chemical shifts using TALOS (49). Distance restraints were obtained from NOE intensities corrected for multiplicity of the ^{1}H spins. NOE connectivities were categorized into three classes (50). Class I contains all intra-residue H^N-H^{α} and all intra-residue, sequential, and medium range H^{β}-H^X NOEs, where X is not a methyl proton. Class III contains all NOEs involving a methyl group, and class II includes all other NOEs. A calibration factor, k_I, was obtained by equating the average class I intensity to 3.4 Å. The class II calibration factor $k_{II} = k_I/2.4^2$. The class III calibration factor $k_{III} = k_{II}/2$. Class I was averaged with a ⅙ order exponent, whereas classes II and III were averaged using a ¼ exponent (50, 51). A standard 10% error term was applied to the upper bound of each restraint. All distances were constrained to the range (1.8, 5.5 Å). Pseudo atom corrections were applied to upper distance restraints for geometric considerations (52).

The ^{1}H,^{15}N, ^{15}N-$^{13}C'$, and $^1H^{\alpha}$-$^{13}C^{\alpha}$ residual dipolar coupling constants were included in the structure calculations. The residual dipolar coupling magnitude and rhombicity were set to −12.5 Hz and 0.55, respectively, during the initial minimization and were refined in the final all-atom minimization. The final average residual dipolar coupling magnitude and rhombicity are −12.8 ± 0.23 Hz and Rh = 0.56 ± 0.01, respectively, for the 200 conformers.

Structural quality statistics refer to residues Leu-1790—Glu-1868 of the 15 lowest-energy structures of 200 total structures calculated. NOE completeness was determined with aqua3.2 (53). The Pearson correlation coefficient (R) and the quality factor (Q) were computed with PALES (54) from 64 C'-C^{α} dipolar couplings that were not included in the structure calculation. MolProbity scores were calculated for the lowest energy structure (55). Average root mean square deviation values were calculated to the average coordinates with VMD (56). Interhelical distances and angles (rounded to the nearest degree) were computed using *interhlx*.[6] Structural alignments were performed with CE (57), and structure figures were prepared with VMD (56) and MOLMOL (58).

RESULTS

The isolated $Na_V1.2$ CTD (1777–1882) and $Na_V1.5$ CTD (1773–1878) constructs each contain the region just after their respective predicted IVS6 transmembrane helix and extend to a region highly conserved among all VGSCs just before the IQ

[6] K. Yap, University of Toronto.

motif. Assignments of ^1H,^{15}N resonances for the $Na_V1.2$ CTD and the $Na_V1.5$ CTD are, respectively, 99 and 97% complete. Notably, Asn-1835 could not be assigned in the ^1H,^{15}N HSQC of $Na_V1.2$. The resonances for Asn-1831 (the homologue of Asn-1835) and Gln-1832 were not assigned, and the resonance for Ile-1833 appears broadened in ^1H,^{15}N HSQC of $Na_V1.5$. Moreover, homologous resonances Leu-1855 in $Na_V1.2$ and Met-1851 in $Na_V1.5$ have liminal intensities in ^1H,^{15}N HSQC spectra. These observations suggest conserved dynamics between isoforms. For the Nav1.2 CTD (1777–1882), $^{13}C^{\alpha}$ and $^{13}C^{\beta}$ assignments are 100% complete, $^{13}C'$ assignments are 97.1% complete, ^1H aromatic assignments are 89.1% complete, and non-aromatic ^1H assignments are 97.7% complete. The $Na_V1.2$ CTD construct contains six proline residues, of which Pro-1789, Pro-1807, Pro-1827, and Pro-1845 are in a *trans* conformation, whereas Pro-1828 and Pro-1834 are in a *cis* conformation. The *cis* conformation is evidenced by stronger X-Pro H^{α}-H^{α} than X-Pro H^{α}-H^{δ} NOE contacts and differences of C^{β}-C^{γ} chemical shifts of 9.4 and 8.5 ppm, respectively (59, 60). Medium range ^1H-^1H NOEs, steady-state $\{^1H\}$-^{15}N NOE, and $^{13}C^{\alpha}$ secondary chemical shifts for $Na_V1.2$ indicate that the CTD forms a well folded domain between residues Leu-1790 and Glu-1868, with a less well ordered region between residues Ser-1869 and Arg-1882 and a disordered N-terminal region between residues Gly-1777 and Pro-1789 (Fig. 1 and supplemental Fig. S1). Secondary chemical shifts indicate that the $Na_V1.5$ CTD has a similar secondary structural architecture as $Na_V1.2$ CTD (Fig. 1*C*).

The structure of $Na_V1.2$ CTD is presented in Fig. 2 and supplemental Fig. S1 with statistical details of the calculation presented in Table 1. The structure contains four α-helices and two short anti-parallel β-strands, consistent with homology models based on structures of paired EF-hand domains (25, 26). Comparison of interhelical angles of helices I and II of $Na_V1.2$ CTD and the N-terminal lobe of the prototypical EF-hand protein calmodulin suggests that the isolated $Na_V1.2$ CTD most closely resembles the canonical apoEF-hand conformation (Fig. 3*D* and Table 2). The hydrophobic interface between helices I and IV predicted through mutational analysis (27) is observed with direct NOE contacts between residues Phe-1795, Phe-1798, and Tyr-1799 in helix I and Leu-1855, Ile-1857, and Leu-1858 in helix IV.

Helices I and IV contribute to the hydrophobic core of the protein, with a majority of aromatic side chains contributed from helix I. The segments between Gln-1811—Glu-1814 and Arg-1851—His-1853 participate in an anti-parallel β-sheet. An additional anti-parallel β-sheet contribution from residues Met-1846—Val-1847 is not present in all conformers of the structural ensemble. The helix II-III interhelical segment, delimited by two *cis* proline residues, Pro-1828 and Pro-1834, is well ordered in the structural ensemble. The conformation of residues Asp-1826—Leu-1829 is consistent with a type VI tight-turn (61), also called a $\beta\alpha_R$ turn (62). The unique di-proline-leucine motif, Pro-1827—Leu-1829 extends the helix II-III interhelical segment by forming a small handle at the base of helix II (Figs. 3, *D* and *E*). The absence of long-range NOE contacts for residues Ser-1848 and Gly-1849 is represented by disorder of this region in the ensemble.

The segment from residues Ser-1869 to Arg-1882 is predicted to have residual helical content based on secondary ^{13}C chemical shifts and characteristic $d_{\alpha N}(i, i+3)$ and $d_{\alpha}\beta(i, i+3)$ NOEs (Fig. 1). A short helix V is observed in the final ensemble extending from Gly-1870 to Arg-1876 with a backbone root mean square deviation of 0.59 Å when superposed on itself (supplemental Fig. S1). However, the reduced magnitudes of the secondary ^{13}C chemical shifts and the $\{^1H\}$-^{15}N NOEs for helix V compared with helices I to IV, suggest that the helical conformation is not fully populated in solution. Furthermore, helix V does not exhibit residual dipolar couplings or long-range NOE contacts and, hence, is not well defined relative to the core EF-hand domain structure (supplemental Fig. S1). Additional interactions present in longer constructs of the CTD or in complexes with other components of the VGSC may stabilize helix V.

Binding of Ca^{2+} by the $Na_V1.2$ (1777–1882) and $Na_V1.5$ (1773–1878) CTDs was assessed by monitoring ^1H,^{15}N chemical shifts as a function of Ca^{2+} concentration (0–4.5 mM). Chemical shift perturbations exhibit titration behavior suggesting that the interaction occurs on a fast-exchange timescale with equilibrium constants of 1.65 ± 0.03 mM for $Na_V1.2$ CTD and 3.28 ± 0.13 mM for $Na_V1.5$ CTD (Fig. 3 and supplemental Fig. S2), consistent with a previous report for the $Na_V1.5$ CTD (33). However, resonance assignments were not obtained previously, and the structure of $Na_V1.2$ CTD now reveals that chemical shift perturbations >0.05 ppm are localized to residues in the N terminus of helix I, the linker between helices II and III, the C terminus of helix IV and the partially structured helix V. Thus, this weak Ca^{2+} binding site is distal to the canonical EF-hand loop motifs. In contrast, the average chemical shift change between the end points of the titration is <0.01 ppm in the N-terminal EF-hand loop (residues 1806–1817) and in the C-terminal EF-hand loop (residues 1842–1853) for the $Na_V1.2$ CTD. Respective values <0.02 ppm were obtained for corresponding residues 1802–1813 and 1832–1849 in the $Na_V1.5$ CTD. In comparison, the average chemical shift changes of the N-terminal EF-hand loop between apoCa^{2+} and Ca^{2+}-loaded calmodulin are 0.59 and 0.65 ppm in the N-terminal and C-terminal domains, respectively (63, 64). In particular, canonical Ca^{2+} binding by an EF-hand would require coordination of a Ca^{2+} atom by the backbone carbonyl atoms of Phe-1812 in $Na_V1.2$ and Phe-1808 in $Na_V1.5$, leading to significant chemical shift changes for inter-residual and sequential amide resonances (65, 66). In opposition, chemical shift changes less than 0.02 ppm were observed for backbone amide resonances for residues Phe-1812–Ile-1813 and Phe-1808—Ile-1809 of $Na_V1.2$ and $Na_V1.5$, respectively (Fig. 3). A structure-based sequence alignment of calmodulin and $Na_V1.2$ and a comparison of Ca^{2+}-induced chemical shift changes are shown in supplemental Fig. S3.

DISCUSSION

The solution structure determined by NMR spectroscopy for the $Na_V1.2$ CTD (1777–1882) exhibits a core-ordered domain from residues Leu-1790 to Glu-1868, with four α-helices and two short anti-parallel β-strands arranged in tandem helix-sheet-helix motifs characteristic of paired EF-hand domains.

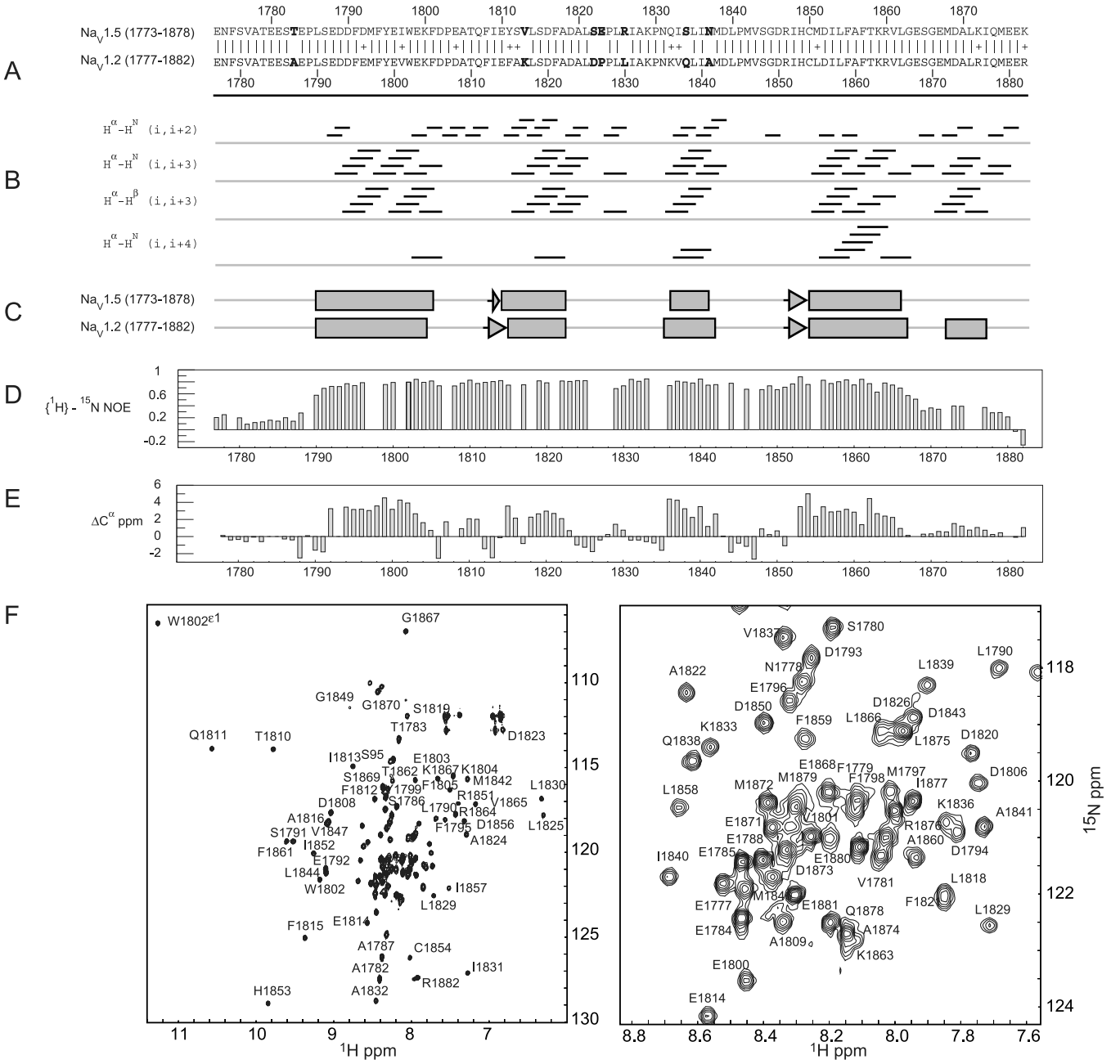

FIGURE 1. **Sequence alignments and NMR data for $Na_V1.2$ and $Na_V1.5$ CTDs.** *A*, sequence alignment of $Na_V1.2$ (1777–1882) and $Na_V1.5$ (1773–1879) CTDs, with 83% identity and 93% similarity. Non-conservative substitutions are shown in *bold type*. *B*, medium range ^{1}H-^{1}H NOEs. *C*, secondary structure elements predicted from chemical shifts using TALOS (49) are shown as *bars* for α-helices and *arrows* for β-strands. {^{1}H}-^{15}N steady-state NOE (*D*) and secondary $^{13}C^{\alpha}$ chemical shifts for $Na_V1.2$ CTD (*E*) indicate a well folded domain encompassing residues Leu-1790—Glu-1868. *F*, ^{1}H,^{15}N HSQC (*right panel*) with expansion of the central region (*left panel*) of $Na_V1.2$ (1777–1882). The W1802$^{\epsilon 1}$ resonance is aliased in the ^{15}N dimension from 131.5 ppm.

Structural alignment of the $Na_V1.2$ CTD and calmodulin reveals that the structure is more similar to apo-Ca^{2+} calmodulin than to peptide target and/or Ca^{2+}-loaded calmodulin. The $Na_V1.5$ CTD (1773–1878), which shares 83% identity with the $Na_V1.2$ CTD, adopts a similar secondary structure and, likely, tertiary structure.

Titrations monitored by NMR chemical shift perturbations demonstrate that the canonical EF-hand loops of the $Na_V1.2$ CTD (1777–1882) and $Na_V1.5$ CTD (1773–1878) do not bind Ca^{2+}; rather, Ca^{2+} binds weakly at a site distal to the canonical loops near the N terminus of helix I, the linker between helices II and III, the C terminus of helix IV, and the partially structured helix V. The high resolution crystal structure of calmodulin identified an additional Ca^{2+} binding site in the homologous region corresponding to the helix II-III linker, but the authors judged this site to be non-physiological (67).

A structure-based sequence alignment with calmodulin also suggests that the canonical EF-hand loops of $Na_V1.2$ CTD do not bind Ca^{2+} (Table 3, Figs. 2, *D* and *E*, and supplemental Fig. S3). Chelation of Ca^{2+} requires an acidic residue, such as Glu or Asp, at sequence position 1817, corresponding to position 12 in a canonical EF-hand calcium binding motif (68), rather than the

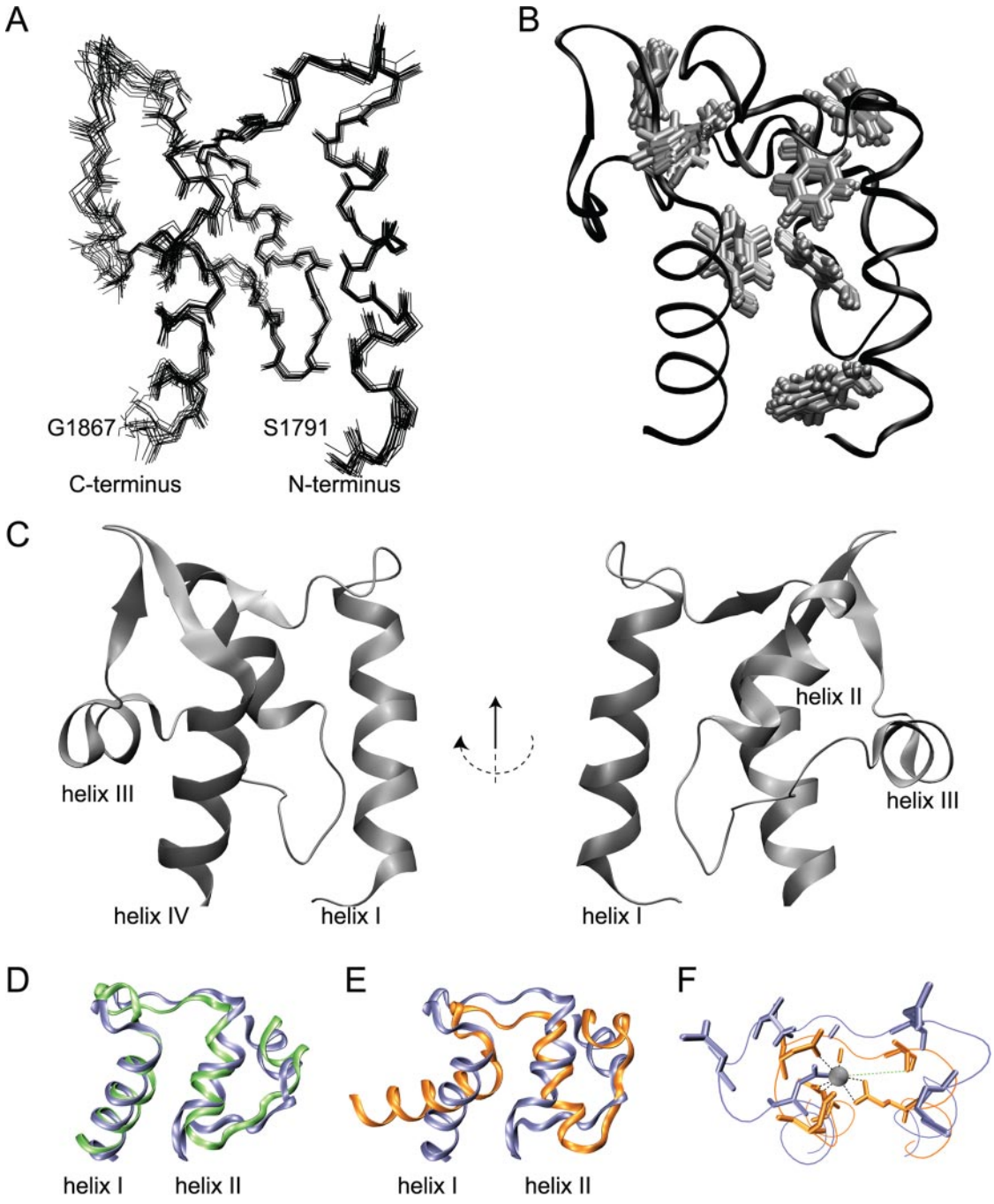

FIGURE 2. **Solution structure of the ordered core EF-hand motif of the $Na_V1.2$ CTD, residues Leu-1790–Glu-1868.** Structural statistics are presented in Table 1; the structure of the construct from residues Gly-1777 to Arg-1882, including the N- and C-terminal regions, is shown in supplemental Fig. S1. Traces through the backbone heavy atoms of the 15 lowest energy conformers described in Table 1 are superposed in *panel A*. Phenylalanine side chains are superposed in *panel B*. Phe-1859 is not shown because the aromatic chain is not well ordered in the ensemble. A *ribbon* diagram of the lowest-energy structure is presented in *panel C*. The structural alignment of the N-terminal EF-hand motifs of $Na_V1.2$ (*blue ribbon*) and apoCa^{2+} calmodulin PDB code 1CFD (*green ribbon*) is shown in *panel D*. The structural alignments to Ca^{2+}-bound calmodulin PDB code 1EXR (*orange ribbon*) is shown in *panel E*. Pentagonal bipyrimidal coordination (*dashed lines*) of calcium by the N-terminal calmodulin (PDB code 1EXR) EF-Hand (*orange*) is shown with the corresponding residues of Nav1.2 in *panel F*. Coordination by T28 (*green dashed line*) occurs through a water molecule.

Lys residue present in $Na_V1.2$. Mutation of the corresponding residue, Glu to Lys, in *Drosophila melanogaster* calmodulin abolishes Ca^{2+} binding, although this mutation may mimic a Ca^{2+}-bound state in the context of certain targets (69, 70). Lys is found at position 12 in the non-canonical Ca^{2+} binding loop of scallop myosin essential light chain; however, coordination of Ca^{2+} is accomplished by an acidic residue at position −2, the backbone carbonyl group at position +2, and a water molecule (71). In $Na_V1.2$ the residue at position +2 is Pro, and the residues at positions −3 and −2 are Glu and Lys. The latter two residues have chemical shift changes less than 0.05 ppm after the addition of 4.5 mM Ca^{2+}.

Higher affinity Ca^{2+} binding has been reported for longer constructs of $Na_V1.5$ CTD, residues 1773–1920 and residues

TABLE 1

Structural statistics for $Na_V1.2$ CTD

Quality statistics are given for residues Leu-1790—Glyu-1868 of the 15 lowest energy structures out of 200 total structures calculated. Errors shown are S.D. for the ensemble. r.m.s.d., root mean square deviation.

Quantity	Value
Unique NOE distance restraints	1772
Intra-residual	699
Sequential	442
Medium range ($2 \leq i \leq 5$)	321
Long range ($i > 5$)	310
Residual violations >0.3 Å per structure ($n = 15$)	1.2 ± 1.1
Maximum violation (Å)	0.27 ± 0.2
NOE completeness per shell	
2.0-2.5 Å (%)	87
2.5-3.0 Å (%)	69
3.0-3.5 Å (%)	57
3.5-4.0 Å (%)	44
TALOS dihedral restraints (ϕ, ψ)	65, 65
Residual dipolar coupling restraints	
H-N	41
N-C′	64
H^{α}-C^{α}	44
R-value; Q-factor (64 C′-C^{α} couplings)	0.93 ± 0.02; 0.38 ± 0.05
PROCHECK	
Most favored (%)	82.2 ± 1.6
Allowed (%)	15.8 ± 1.7
Generously allowed (%)	1.41 ± 0.8
Disallowed (%)	0.5 ± 0.9
MolProbity score; all-atom clash score (percentiles)	3.09 (20th); 20.33 (31th)
Average backbone r.m.s.d. (Å)	0.80
Average all atom r.m.s.d. (Å)	1.29

1773–1925 that include the IQ motif, and binding is abolished by mutation of the IQ motif (33). However, the resonance assignments obtained for $Na_V1.5$ indicate that chemical shift perturbations for key EF-hand canonical loop residues Phe-1808—Ile-1809 are not larger in these longer constructs (comparing the *inset* of Fig. 3*B* with supplemental Fig. 5*D* of Ref. 33), suggesting that higher affinity binding of Ca^{2+} also does not involve the canonical EF-hand loops.

The solution structure of $Na_V1.2$ CTD can be used to predict the effect(s) of clinical mutations in VGSCs (Fig. 4) because of the high degree of homology between VGSC CTDs. Generally, clinically significant mutations that map in the CTD can be divided into two classes, with some overlap for several sites (supplemental Table SI). Mutations in $Na_v1.5$ associated with the Long QT variant 3 (LQT3) cardiac arrhythmia phenotype and a subset of mutations in $Na_v1.1$ associated with certain epilepsy syndromes lead to persistent current during maintained depolarization. A second set of mutations in $Na_v1.1$ associated with multiple epilepsy syndromes and mutations in $Na_v1.5$ associated with the Brugada syndrome cardiac arrhythmia led to decreased current, resulting from loss of function or enhanced inactivation kinetics.

Multiple mutations in $Na_V1.1$ and $Na_V1.5$ associated with an increased persistent current are observed at positions clustering in the corresponding helix I of the $Na_V1.2$ CTD. The F1808L

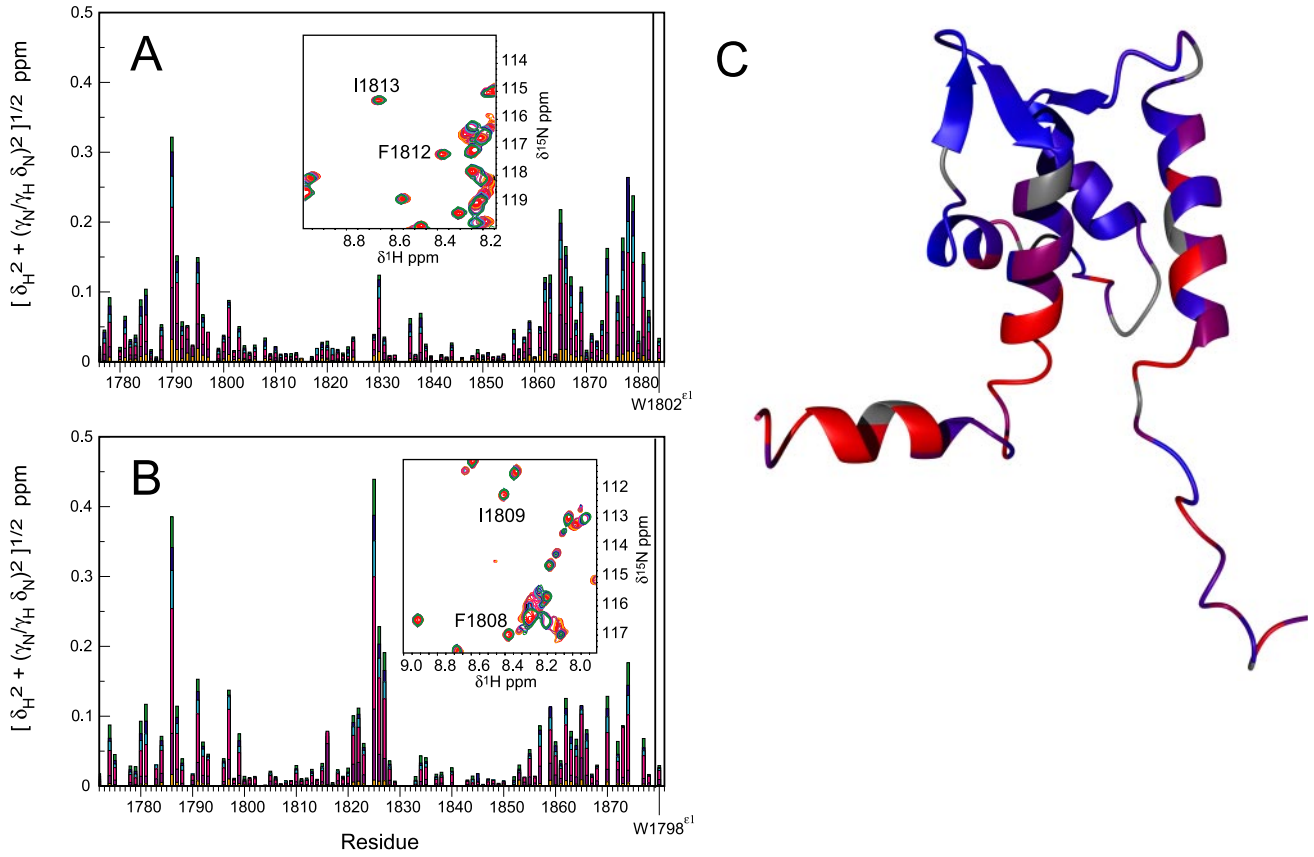

FIGURE 3. Ca^{2+} titration of $Na_V1.2$ (1777–1882) (*panel A*) and $Na_V1.5$ (1773–1878) (*panel B*). The plots show joint ^1H,^{15}N chemical shift deviations from resonance assignments in 0 mM Ca^{2+}. The titration was performed by serial addition of Ca^{2+} obtaining the following concentrations: 0 (*red*), 0.1 (*orange*), 0.5 (*maroon*), 1.5 (*magenta*), 2.5 (*cyan*), 3.5 (*blue*), and 4.5 mM (*green*) for $Na_V1.2$ (*panel A*) and (0 (*red*), 0.1 (*orange*), 0.5 (*maroon*), 2.5 (*magenta*), 3.5 (*cyan*), 4.5 (*blue*), and 5.5 mM (*green*) for $Na_V1.5$. *Insets* show resonances Phe-1812—Ile-1813 and Phe-1808—Ile-1809 for $Na_V1.2$ and $Na_V1.5$, respectively. Titration curves are shown in supplemental Fig. S2. In *panel C* the joint ^1H,^{15}N chemical shift changes for $Na_V1.2$ (1777–1882) at 4.5 mM Ca^{2+} are mapped onto the lowest energy structure, interpolated between 0 ppm (*blue*) and 0.1 ppm (*red*).

TABLE 2

Comparison of helix orientations in EF-hand proteins

Interhelical angles are shown in degrees with interhelical distances shown in Å in parentheses. Calculations refer to the following structures. Ca-CaM is Ca^{2+}-loaded target-free calmodulin (PDB code 1EXR, 1.00 Å) (67), IQ-Ca-CaM is Ca^{2+}-loaded calmodulin bound to the voltage-gated Ca^{2+} channel $Ca_V1.2$ IQ-motif (PDB code 2F3Y, 1.45 Å) (81), and apoCaM is apoCa^{2+} target-free calmodulin (PDB code 1CFD, NMR) (82), with helix I defined as residues 6–18, helix II as residues 29–38, helix III as residues 45–54, and helix IV as residues 65–74. Interhelical angles for the $Na_V1.2$ CTD are the averages with S.D. for the structural ensemble.

Molecule	Helix II	Helix III	Helix IV
Helix I			
Ca-CaM	85 (20.4)	−134 (25.5)	91 (14.6)
IQ-Ca-CaM	92 (18.3)	−161 (21.9)	117 (10.1)
ApoCaM	136 (12.9)	−93 (21.2)	126 (11.9)
$Na_V1.2$ CTD	152 ± 2 (10.9 ± 0.1)	−103 ± 6 (20.9 ± 0.3)	143 ± 1 (15.7 ± 0.2)
Helix II			
Ca-CaM		83 (10.1)	−20 (16.7)
IQ-Ca-CaM		107 (11.2)	−41 (18.6)
ApoCaM		125 (11.9)	−49 (12.9)
$Na_V1.2$ CTD		100 ± 5 (10.8 ± 0.4)	−46 ± 2 (13.4 ± 0.1)
Helix III			
Ca-CaM			65 (15.3)
IQ-Ca-CaM			80 (16.5)
ApoCaM			129 (14.1)
$Na_V1.2$ CTD			98 ± 6 (14.4 ± 0.4)

TABLE 3

Structure-based sequence alignment

N-terminal calcium binding loop of CaM aligned with the respective N-terminal EF-hand loop sequences from $Na_V1.2$ and $Na_V1.5$ CTD sequences, based on a structural alignment between apo-CaM and the $Na_V1.2$ CTD.

Ca^{2+} coordination	X		Y		Z		−Y		−X			−Z
Position	1	2	3	4	5	6	7	8	9	10	11	12
$Na_V1.2$	D	P	D	A	T	Q	F	I	E	F	A	K
$Na_V1.5$	D	P	E	A	T	Q	F	I	E	Y	S	V
CaM	D	K	D	G	D	G	T	I	T	T	K	E

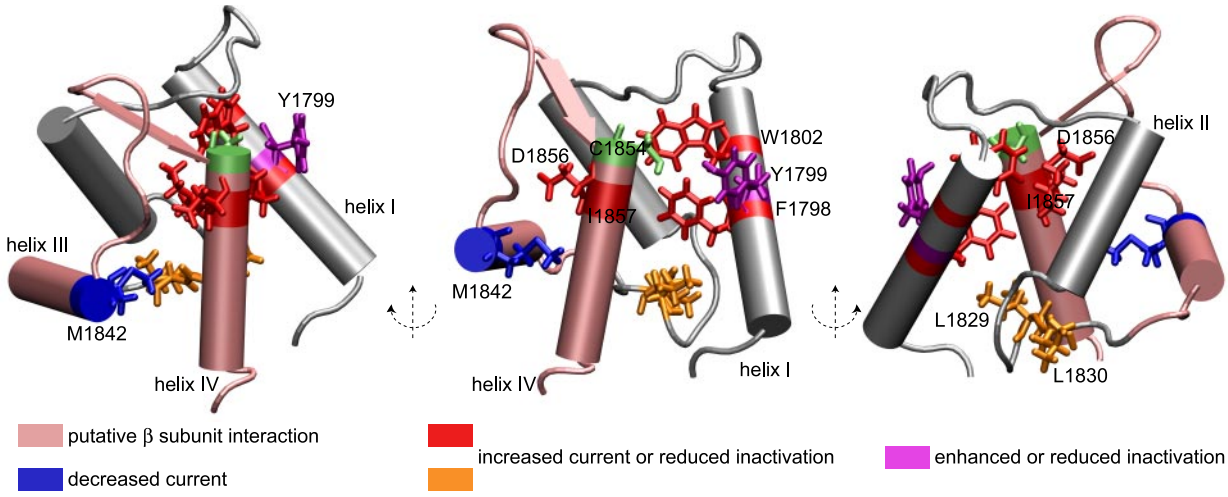

FIGURE 4. **NMR structure of $Na_V1.2$ (1777–1882) CTD with functionally significant mutations observed in Nav1.1 and Nav1.5 channels.** The lowest energy structure of the calculated ensemble is shown. Mutations leading to persistent current cluster in helices I and IV (show in *red*) and the helix II-III segment (shown in *orange*), whereas a position (1842) at which mutation (M1852T) leads to decreased current is shown in *blue*. Position 1799 at which substitutions lead to increased or decreased inactivation is shown in *violet*, and residue Cys-1854 is shown in *green*. The putative *β* subunit interaction site is shown in *pink*.

mutation associated with intractable childhood epilepsy with generalized tonic clonic seizures in $Na_V1.1$ may destabilize the protein core because the aromatic ring of Phe-1798 in $Na_V1.2$ contacts residues in helix IV and the helix II-III interhelical segment (4, 72). The insertion of an Asp residue at position 1795, Y1795insD, leads to both LQT3 and Brugada syndrome phenotypes in $Na_V1.5$ and potentially disrupts helix I by shifting the register of helical interactions (73).

Substitution at position Tyr-1795 in $Na_V1.5$ differentially leads to decreased inactivation for Y1795C in LQT3 or enhanced inactivation kinetics for Y1795H in Brugada syndrome, whereas both substitutions lead to sustained current during maintained depolarization and negative shift of voltage dependence of inactivation (27, 74). The Y1795C mutation has been suggested to form an intra-molecular disulfide bond with Cys-1850 in $Na_V1.5$ (32). The average C^{β}-C^{β} distance of the corresponding residues in the $Na_V1.2$ CTD structural ensemble is 9.6 ± 0.4 Å. The C^{β}-C^{β} distance in cysteine disulfide bonds ranges from 3.4 to 4 Å (75); thus, the proposed disulfide bond may be intermolecular or require structural rearrangement on the order of several angstroms between helix I and IV (Fig. 4) if it is formed. Furthermore, although Tyr-1795 in $Na_V1.5$ was predicted to contribute to the hydrophobic interface between helices I and IV (27), the corresponding residue Tyr-1799 in

$Na_V1.2$ is found in a position closer to the surface; the total side-chain exposed surface area is 103 ± 10 Å^2 for the conformers in Table 1. Hence, mutations at position Tyr-1799 may also affect interactions with other components of the intact channel. On the other hand, the conserved Trp-1802, corresponding to Trp-1798 in Nav1.5, is not completely accessible as observed previously (27); the total side-chain exposed surface area is 9 ± 5 Å^2 for the conformers in Table 1.

The L1825P mutation associated with LQT3 and the R1826H mutation associated with sudden infant death syndrome in $Na_V1.5$ occurs in the helix II-III interhelical segment (76, 77). The L1825P mutation results in significant persistent current and slows kinetics of inactivation. Interestingly, the L1825P mutation in $Na_V1.5$ introduces a di-proline motif, as is observed in wild type $Na_V1.1$, $Na_V1.2$, $Na_V1.3$, and $Na_V1.7$, but shifted by one residue. The residue corresponding to Arg-1826 in $Na_V1.2$ is Leu-1830, and some local difference in conformation probably exists. Like L1825P, the R1826H mutation leads to persistent current in $Na_V1.5$, further suggesting that the helix II-III interhelical segment is critical to channel inactivation.

Two mutations implicated in interactions with other components of the sodium channel cluster in helices III and IV. The D1866Y mutation in $Na_V1.1$, associated with generalized epilepsy and febrile seizures plus, leads to persistent current and decreased fast inactivation kinetics in the presence of the β subunit (78). The corresponding position Asp-1856 in $Na_V1.2$ is at the start of helix IV and may disturb a putative surface for interaction with the β subunit, as interaction with the β1 subunit and the CTD is suggested to occur through the second helix-sheet-helix motif by yeast-two-hybrid analysis of residues Lys-1846—Arg-1886 in $Na_V1.1$ (78). Additionally, the M1852T mutation in $Na_V1.1$, also associated with generalized epilepsy and febrile seizures plus, results in decreased current (loss of function). This phenotype can be rescued by co-expression with β subunits or calmodulin (79). Proposed to be a folding/trafficking defect, this mutation may destabilize helix III, further suggesting that the second helix-sheet-helix motif may be important for interaction with other components of the sodium channel.

The notable exception to the above patterns is the LQT3 mutation D1790G in $Na_V1.5$, resulting in a relative negative shift in the voltage dependence of inactivation in the presence of the β subunit (19, 80). D1790G corresponds to position D1794 in helix I of Nav1.2 and may disrupt the helix by introduction of a glycine residue, with the effect of propagating to helices III and IV.

The mechanisms and extent of Na_V1 CTD function in binding the IQ motif and the specific role of calmodulin as well as Ca^{2+} in multiple phases of inactivation remains to be elaborated. Interactions with the IQ motif may be more complicated than present models and may involve additional components (33). Previous evidence shows that Ca^{2+}-dependent regulation of VGSC is mediated by calmodulin (31), with the exact mode of interaction yet to be determined. The solution structure of the $Na_V1.2$ C-terminal domain and chemical shift assignments of $Na_V1.5$ (1773–1878) are initial steps in elucidating the mechanism of inactivation, extended to other isoforms by virtue of high degrees of homology. The current work provides a template to begin probing specific interactions between the C-terminal domain and other components that play a role in inactivation of voltage-gated sodium channels.

Acknowledgment—We thank Mary Ann Gawinowicz (Columbia University Protein Core Facility) for N-terminal sequencing.

REFERENCES

1. Brugada, J., Brugada, P., and Brugada, R. (1999) *Europace* **1,** 156–166
2. Terrenoire, C., Simhaee, D., and Kass, R. S. (2007) *J. Cardiovasc. Electrophysiol.* **18,** 900–905
3. Alekov, A. K., Rahman, M., Mitrovic, N., Lehmann-Horn, F., and Lerche, H. (2001) *Eur. J. Neurosci.* **13,** 2171–2176
4. Fujiwara, T., Sugawara, T., Mazaki-Miyazaki, E., Takahashi, Y., Fukushima, K., Watanabe, M., Hara, K., Morikawa, T., Yagi, K., Yamakawa, K., and Inoue, Y. (2003) *Brain* **126,** 531–546
5. Abriel, H., and Kass, R. S. (2005) *Trends Cardiovasc. Med.* **15,** 35–40
6. Pitt, G. S. (2007) *Cardiovasc. Res.* **73,** 641–647
7. Goldin, A. L., Barchi, R. L., Caldwell, J. H., Hofmann, F., Howe, J. R., Hunter, J. C., Kallen, R. G., Mandel, G., Meisler, M. H., Netter, Y. B., Noda, M., Tamkun, M. M., Waxman, S. G., Wood, J. N., and Catterall, W. A. (2000) *Neuron* **28,** 365–368
8. The, Y. K., Fernandes, J., Popa, M. O., Alekov, A. K., Timmer, J., and Lerche, H. (2006) *Biophys. J.* **90,** 3511–3522
9. Goldin, A. L. (2003) *Curr. Opin. Neurobiol.* **13,** 284–290
10. Tikhonov, D. B., and Zhorov, B. S. (2007) *Biophys. J.* **93,** 1557–1570
11. Qu, Y. S., Isom, L. L., Westenbroek, R. E., Rogers, J. C., Tanada, T. N., McCormick, K. A., Scheuer, T., and Catterall, W. A. (1995) *J. Biol. Chem.* **270,** 25696–25701
12. Tan, H. L., Kupershmidt, S., Zhang, R., Stepanovic, S., Roden, D. M., Wilde, A. A. M., Anderson, M. E., and Balser, J. R. (2002) *Nature* **415,** 442–447
13. Ulbricht, W. (2005) *Physiol. Rev.* **85,** 1271–1301
14. Casini, S., Tan, H. L., Bhuiyan, Z. A., Bezzina, C. R., Barnett, P., Cerbai, E., Mugelli, A., Wilde, A. A. M., and Veldkamp, M. W. (2007) *Cardiovasc. Res.* **76,** 418–429
15. Hilber, K., Sandtner, W., Kudlacek, O., Glaaser, I. W., Weisz, E., Kyle, J. W., French, R. J., Fozzard, H. A., Dudley, S. C., and Todt, H. (2001) *J. Biol. Chem.* **276,** 27831–27839
16. Vilin, Y. Y., Makita, N., George, A. L., and Ruben, P. C. (1999) *Biophys. J.* **77,** 1384–1393
17. Stuhmer, W., Conti, F., Suzuki, H., Wang, X. D., Noda, M., Yahagi, N., Kubo, H., and Numa, S. (1989) *Nature* **339,** 597–603
18. Rohl, C. A., Boeckman, F. A., Baker, C., Scheuer, T., Catterall, W. A., and Klevit, R. E. (1999) *Biochemistry* **38,** 855–861
19. An, R. H., Wang, X. L., Kerem, B., Benhorin, J., Medina, A., Goldmit, M., and Kass, R. S. (1998) *Circ. Res.* **83,** 141–146
20. Deschenes, I., Trottler, E., and Chahine, M. (1999) *Circulation* **100,** 278–279
21. Motoike, H. K., Liu, H. J., Glaaser, I. W., Yang, A. S., Tateyama, M., and Kass, R. S. (2004) *J. Gen. Physiol.* **123,** 155–165
22. Wang, D. W., Makita, N., Kitabatake, A., Balser, J. R., and George, A. L. (2000) *Circ. Res.* **87,** 37–43
23. Babitch, J. A., and Anthony, F. A. (1987) *J. Theor. Biol.* **127,** 451–459
24. Babitch, J. (1990) *Nature* **346,** 321–322
25. Cormier, J. W., Rivolta, I., Tateyama, M., Yang, A. S., and Kass, R. S. (2002) *J. Biol. Chem.* **277,** 9233–9241
26. Wingo, T. L., Shah, V. N., Anderson, M. E., Lybrand, T. P., Chazin, W. J., and Balser, J. R. (2004) *Nat. Struct. Mol. Biol.* **11,** 219–225
27. Glaaser, I. W., Bankston, J. R., Liu, H. J., Tateyama, M., and Kass, R. S. (2006) *J. Biol. Chem.* **281,** 24015–24023
28. Mori, M., Konno, T., Ozawa, T., Murata, M., Imoto, K., and Nagayama, K. (2000) *Biochemistry* **39,** 1316–1323
29. Young, K. A., and Caldwell, J. H. (2005) *J. Physiol.* (*Lond.*) **565,** 349–370
30. Biswas, S., Deschenes, I., DiSilvestre, D., Tian, Y., Halperin, V. L., and Tomaselli, G. F. (2008) *J. Gen. Physiol.* **131,** 197–209

31. Kim, J., Ghosh, S., Liu, H. J., Tateyama, M., Kass, R. S., and Pitt, G. S. (2004) *J. Biol. Chem.* **279,** 45004–45012
32. Tateyama, M., Liu, H., Yang, A. S., Cormier, J. W., and Kass, R. S. (2004) *Biophys. J.* **86,** 1843–1851
33. Shah, V. N., Wingo, T. L., Weiss, K. L., Williams, C. K., Balser, J. R., and Chazin, W. J. (2006) *Proc. Natl. Acad. Sci. U. S. A.* **103,** 3592–3597
34. Pitt, B., and Pitt, G. S. (2007) *Circulation* **115,** 2976–2982
35. Maniatis, T., Fritsch, E. F., and Sambrook, J. (1989) *Molecular Cloning: A Laboratory Manual*, Cold Spring Harbor Laboratory Press, Cold Spring Harbor, NY
36. Tatusova, T. A., and Madden, T. L. (1999) *FEMS Microbiol. Lett.* **174,** 247–250
37. Findeisen, M., Brand, T., and Berger, S. (2007) *Magn. Reson. Chem.* **45,** 175–178
38. Cavanagh, J., Fairbrother, W., Palmer, A. I., Rance, M., and Skelton, N. (2007) *Protein NMR Spectroscopy: Principles and Practice*, 2nd Ed., Academic Press, Boston, MA
39. Neri, D., Szyperski, T., Otting, G., Senn, H., and Wüthrich, K. (1989) *Biochemistry* **28,** 7510–7516
40. Ottiger, M., Delaglio, F., and Bax, A. (1998) *J. Magn. Reson.* **131,** 373–378
41. Permi, P., Rosevear, P. R., and Annila, A. (2000) *J. Biomol. NMR* **17,** 43–54
42. Chou, J. J., Delaglio, F., and Bax, A. (2000) *J. Biomol. NMR* **18,** 101–105
43. Cicero, D. O., Contessa, G. M., Paci, M., and Bazzo, R. (2006) *J. Magn. Reson.* **180,** 222–228
44. Markley, J. L., Bax, A., Arata, Y., Hilbers, C. W., Kaptein, R., Sykes, B. D., Wright, P. E., and Wüthrich, K. (1998) *J. Biomol. NMR* **12,** 1–23
45. Rieping, W., Habeck, M., Bardiaux, B., Bernard, A., Malliavin, T. E., and Nilges, M. (2007) *Bioinformatics* **23,** 381–382
46. Brunger, A. T., Adams, P. D., Clore, G. M., DeLano, W. L., Gros, P., Grosse-Kunstleve, R. W., Jiang, J. S., Kuszewski, J., Nilges, M., Pannu, N. S., Read, R. J., Rice, L. M., Simonson, T., and Warren, G. L. (1998) *Acta Crystallogr. D Biol. Crystallogr.* **54,** 905–921
47. Schwieters, C. D., Kuszewski, J. J., Tjandra, N., and Clore, G. M. (2003) *J. Magn. Reson.* **160,** 65–73
48. Schwieters, C. D., Kuszewski, J. J., and Clore, G. M. (2006) *Prog. Nucl. Magn. Reson. Spectrosc.* **48,** 47–62
49. Cornilescu, G., Delaglio, F., and Bax, A. (1999) *J. Biomol. NMR* **13,** 289–302
50. Guntert, P., and Wüthrich, K. (1991) *J. Biomol. NMR* **1,** 447–456
51. Mumenthaler, C., Guntert, P., Braun, W., and Wüthrich, K. (1997) *J. Biomol. NMR* **10,** 351–362
52. Fletcher, C. M., Jones, D. N. M., Diamond, R., and Neuhaus, D. (1996) *J. Biomol. NMR* **8,** 292–310
53. Doreleijers, J. F., Raves, M. L., Rullmann, T., and Kaptein, R. (1999) *J. Biomol. NMR* **14,** 123–132
54. Zweckstetter, M., and Bax, A. (2000) *J. Am. Chem. Soc.* **122,** 3791–3792
55. Davis, I. W., Leaver-Fay, A., Chen, V. B., Block, J. N., Kapral, G. J., Wang, X., Murray, L. W., Arendall, W. B., Snoeyink, J., Richardson, J. S., and Richardson, D. C. (2007) *Nucleic Acids Res.* **35,** 375–383
56. Humphrey, W., Dalke, A., and Schulten, K. (1996) *J. Mol. Graph.* **14,** 33–38
57. Shindyalov, I. N., and Bourne, P. E. (1998) *Protein Eng.* **11,** 739–747
58. Koradi, R., Billeter, M., and Wuthrich, K. (1996) *J. Mol. Graph.* **14,** 51–55
59. Wüthrich, K. (1986) *NMR of Proteins and Nucleic Acids*, Wiley, New York
60. Schubert, M., Labudde, D., Oschkinat, H., and Schmieder, P. (2002) *J. Biomol. NMR* **24,** 149–154
61. Chou, K. C. (2000) *Anal. Biochem.* **286,** 1–16
62. Wilmot, C. M., and Thorton, J. M. (1990) *Protein Eng.* **3,** 479–493
63. Ikura, M., Kay, L. E., and Bax, A. (1990) *Biochemistry* **29,** 4659–4667
64. Tjandra, N., Kuboniwa, H., Ren, H., and Bax, A. (1995) *Eur. J. Biochem.* **230,** 1014–1024
65. Biekofsky, R. R., Martin, S. R., Browne, J. P., Bayley, P. M., and Feeney, J. (1998) *Biochemistry* **37,** 7617–7629
66. Xu, X. P., and Case, D. A. (2002) *Biopolymers* **65,** 408–423
67. Wilson, M. A., and Brunger, A. T. (2000) *J. Mol. Biol.* **301,** 1237–1256
68. Gifford, J. L., Walsh, M. P., and Vogel, H. J. (2007) *Biochem. J.* **405,** 199–221
69. Maune, J. F., Klee, C. B., and Beckingham, K. (1992) *J. Biol. Chem.* **267,** 5286–5295
70. Gao, Z. H., Krebs, J., Vanberkum, M. F. A., Tang, W. J., Maune, J. F., Means, A. R., Stull, J. T., and Beckingham, K. (1993) *J. Biol. Chem.* **268,** 20096–20104
71. Houdusse, A., and Cohen, C. (1996) *Structure* **4,** 21–32
72. Rhodes, T. H., Vanoye, C. G., Ohmori, I., Ogiwara, I., Yamakawa, K., and George, A. L. (2005) *J. Physiol.* (*Lond.*) **569,** 433–445
73. Bezzina, C., Veldkamp, M. W., van den Berg, M. P., Postma, A. V., Rook, M. B., Viersma, J. W., van Langen, I. M., Tan-Sindhunata, G., Bink-Boelkens, M. T. E., van der Hout, A. H., Mannens, M., and Wilde, A. A. M. (1999) *Circ. Res.* **85,** 1206–1213
74. Rivolta, I., Abriel, H., Tateyama, M., Liu, H. H., Memmi, M., Vardas, P., Napolitano, C., Priori, S. G., and Kass, R. S. (2001) *J. Biol. Chem.* **276,** 30623–30630
75. Hazes, B., and Dijkstra, B. W. (1988) *Protein Eng.* **2,** 119–125
76. Makita, N., Horie, M., Nakamura, T., Ai, T., Sasaki, K., Yokoi, H., Sakurai, M., Sakuma, I., Otani, H., Sawa, H., and Kitabatake, A. (2002) *Circulation* **106,** 1269–1274
77. Ackerman, M. J., Siu, B. L., Sturner, W. Q., Tester, D. J., Valdivia, C. R., Makielski, J. C., and Towbin, J. A. (2001) *J. Am. Med. Assoc.* **286,** 2264–2269
78. Spampanato, J., Kearney, J. A., de Haan, G., McEwen, D. P., Escayg, A., Aradi, I., MacDonald, B. T., Levin, S. I., Soltesz, I., Benna, P., Montalenti, E., Isom, L. L., Goldin, A. L., and Meisler, M. H. (2004) *J. Neurosci.* **24,** 10022–10034
79. Rusconi, R., Scalmani, P., Cassulini, R. P., Giunti, G., Gambardella, A., Franceschetti, S., Annesi, G., Wanke, E., and Mantegazza, M. (2007) *J. Neurosci.* **27,** 11037–11046
80. Abriel, H., Wehrens, X. H. T., Benhorin, J., Kerem, B., and Kass, R. S. (2000) *Circulation* **102,** 921–925
81. Fallon, J. L., Halling, D. B., Hamilton, S. L., and Quiocho, F. A. (2005) *Structure* **13,** 1881–1886
82. Kuboniwa, H., Tjandra, N., Grzesiek, S., Ren, H., Klee, C. B., and Bax, A. (1995) *Nat. Struct. Biol.* **2,** 768–776